Inorganic Chemistry

Article

pubs.acs.org/IC

Cobalt Corrole Catalyst for Efficient Hydrogen Evolution Reaction from H_2O under Ambient Conditions: Reactivity, Spectroscopy, and Density Functional Theory Calculations

Biswajit Mondal,[†] Kushal Sengupta,[†] Atanu Rana,[†] Atif Mahammed,[‡] Mark Botoshansky,[‡] Somdatta Ghosh Dey,*[,†] Zeev Gross,*[,‡] and Abhishek Dey*[,†]

[†]Department of Inorganic Chemistry, Indian Association for the Cultivation of Science, Kolkata, India 700032

[‡]Schulich Faculty of Chemistry, Technion—Israel Institute of Technology, Haifa 32000, Israel

Supporting Information

ABSTRACT: The feasibility of a hydrogen-based economy relies very much on the availability of catalysts for the hydrogen evolution reaction (HER) that are not based on Pt or other noble elements. Significant breakthroughs have been achieved with certain first row transition metal complexes in terms of low overpotentials and large turnover rates, but the majority of reported work utilized purified and deoxygenated solvents (most commonly mixtures of organic solvents/acids). Realizing that the design of earth abundant metal catalysts that operate under truly ambient conditions remains an unresolved challenge, we have now developed an electronically tuned Co(III) corrole that can catalyze the HER from aqueous sulfuric acid at as low as −0.3 V vs NHE, with a turnover frequency of 600 s^{-1} and $\gg 10^7$ catalytic turnovers. Under aerobic conditions, using H_2O from naturally available sources without any pretreatment, the same complex catalyzes the reduction of H^+ with a Faradaic Yield (FY) of 52%. Density functional theory (DFT) calculations indicate that the electron density on a putative hydride species is delocalized off from the H atom into the macrocycle. This makes the protonation of a $[Co(III)\text{-}H]^-$ species the rate determining step (rds) for the HER consistent with the experimental data.

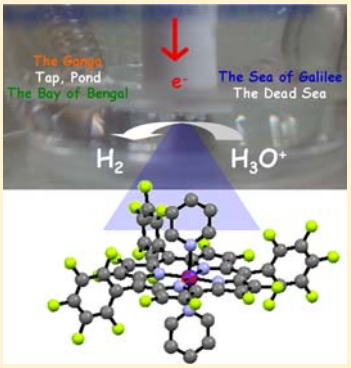

1. INTRODUCTION

Water splitting to its elementals, H_2 and O_2, may be considered the ultimate approach for storing energy in the form of stable yet reactive chemical bonds.[1] Once obtained, the H_2 may be used in fuel cells as a possible clean and sustainable pathway for meeting the ever-increasing global energy need. Many techniques for the production of H_2 from natural gas, methanol, biomass, and other nonrenewable material do exist,[1−8] but its efficient generation from water still remains the crux of a hydrogen-based economy.[1,2] What has held back this development for decades is that efficient catalysts for the hydrogen evolution reaction (HER) are based on expensive and rare noble metals (mainly Pt).[9,10] A practical catalyst must be affordable, operate fast (i.e., large turnover frequencies, TOF) and at low overpotential, and also be able to function under aerobic conditions with large turnover numbers ([mol H_2]/[mol catalyst], TON). Thus there has been a flurry of activity in this area over the past decade, and several catalysts based on first row transition metals have been reported.[11] There are several reports of H_2 generation from organic acids by Fe, Co, and Ni dithiolene and thiolate complexes.[12,13] Recently, a few Mo based catalysts (note that Mo is 100 times more earth abundant than Pt) that can generate H_2 from water have been reported.[14,15] Nevertheless, there is still a lack of an efficient catalyst that works in aqueous medium at low overpotential and under aerobic conditions. One issue that has impeded such developments is the water-insolubility of most of these catalysts, which has been successfully circumvented by absorbing them onto electrodes. Table 1 summarizes literature reports on first-row transition metal catalysts that perform reasonably well in aqueous medium. It reveals that all reported systems operate under anaerobic conditions and in high purity solvent, and also that there is no catalyst that displays all the desired parameters for the HER: high TON, high TOF, and relatively positive onset potential.[14−20] We now show that the tris(5,10,15-pentafluorophenyl)-2,3,7,8,12,13,17,18-octafluorocorrole (Co−F_8) catalyst (Figure 1a) immobilized on graphite electrode can catalyze the HER very efficiently, from water obtained from local sources without requiring pretreatment, and even under aerobic conditions.

2. EXPERIMENTAL DETAILS

1. Materials. Pentafluorobenzaldehyde, dichloro dicyano quinone (DDQ), cobalt acetate [$Co(OAc)_2{\cdot}4H_2O$], octanethiol (C_8SH), potassium hexafluorophosphate (KPF_6), and tetrabutylammonium perchlorate (TBAP) were purchased from Sigma-Aldrich. Di-Sodium hydrogen phosphate dihydrate ($Na_2HPO_4{\cdot}2H_2O$) and sulfuric acid (H_2SO_4, 98%) were purchased from Merck. Edge Plane Graphite (EPG), Au and Ag discs for the Rotating Ring Disc Electrochemistry (RRDE) and Surface Enhanced Resonance Raman Spectroscopy (SERRS) experiments were purchased from Pine Instruments, U.S.A.

Received: January 9, 2013
Published: February 27, 2013

   dx.doi.org/10.1021/ic4000473 | Inorg. Chem. 2013, 52, 3381−3387

Table 1. Reported Non-Platinum Complexes for Electrocatalytic H_2 Production in Aqueous Media

			performance			
catalyst	onset overpotential for H^+ reduction	medium	TON[a]	TOF[a]	atmosphere	reference
Co−F_8	**241 mV**	0.5 M H_2SO_4	**≫10^7**	**600 s^{-1}**	**N_2, as well as aerobic**	this work
Co-pentapyridine	787 mV	pH 7, phosphate buffer	∼10^4	0.3 s^{-1}	N_2	16
molecular MoS_2 catalyst	473 mV	1 M aqueous phosphate buffer (pH 3)	∼10^3	480 s^{-1}	N_2	15
molybdenum-oxo catalyst	517 mV	phosphate buffer (pH 7)	∼10^5	2.4 s^{-1}	N_2	14
cobalt tetraazamacrocycle	500 mV	pH 2.2 phosphate buffer	23	not reported	N_2	17
cobalt tetraimine catalyst	442 mV	aqueous solution pH 2	∼10^5	not reported	N_2	18
cobalt bis(iminopyridine)	782 mV	pH 2 buffer	not reported	2.2 h^{-1}	N_2	19
Co-clathrochelate	591 mV	water containing phosphate buffer	not reported	not reported	N_2	20

[a]Generally calculated at 200−400 mV below the onset potential.

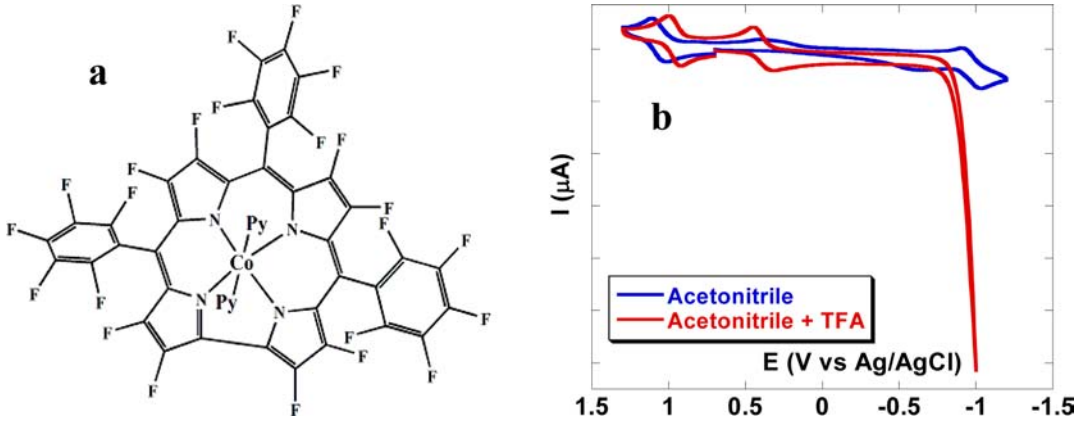

Figure 1. (a) Chemical structure of the bis-pyridine Co−F_8 complex. (b) CV of (pyridine)$_2$Co(III)-F_8 in pure acetonitrile (blue) and in acetonitrile containing 0.13 M TFA (red). Scan rate 50 mV/s, Glassy Carbon (GC) working, Pt counter and Ag/AgCl reference electrode. The redox potential CV in 0.13 M TFA is shifted because of dissociation of the metal-bound pyridine ligands due to protonation.

2. Instrumentation. UV−vis data were taken in Agilent technologies spectrophotometer model 8453 fitted with a diode-array detector. All electrochemical experiments were performed using a CH Instruments (model CHI710D Electrochemical Analyzer). Biopotentiostat, reference electrodes, were purchased from CH Instruments. The RRDE set up from Pine Research Instrumentation (E6 series ChangeDisk tips with AFE6M rotor) was used to obtain the RRDE data. Resonance Raman data were collected using a Trivista 555 spectograph (Princeton Instruments) and using 413.1 nm excitation wavelength from a Kr^+ laser (Coherent, Sabre Innova SBRC-DBW-K). The EPR spectrum was recorded on a JEOL instrument.

3. Synthesis of 2,3,7,8,12,13,17,18-Octafluoro-5,10,15-tris-(pentafluorophenyl)corrole. A 0.5 g portion (4.85 mmol) of 3,4-difluoropyrrole (*1*) was dissolved in 1 mL of CH_2Cl_2 and added to a stirred solution of 400 μL (3.24 mmol) of pentafluorobenzaldehyde and 50 μL of CH_2Cl_2 containing 10% TFA at 50 °C. The mixture was stirred vigorously for 1 h after which 80 mL of CH_2Cl_2 and 0.6 g (2.64 mmol) of DDQ in 1 mL of THF were added, and the mixture was stirred for further 10 min. The solvent was evaporated, and the product was purified by column chromatography on silica gel (eluent, hexanes/CH_2Cl_2 9:1 which was changed to acetone). The fluorescence fraction was collected and further purified on PTLC of silica (eluent, acetone/hexanes 1:1). The spectral properties of the product were consistent with literature data. (*2*) ^{19}F NMR (188 MHz, C_6D_6): δ, ppm= −139.5 (dd, ^3J(F,F) = 24.5 Hz, ^4J(F,F) = 7.7 Hz, 2F; *ortho*-F), −140.0 (dd, ^3J(F,F) = 24.1 Hz, ^4J(F,F) = 7.5 Hz, 4F; *ortho*-F), −154.7 (t, ^3J(F,F) = 20.9 Hz, 2F; *para*-F), −155.3 (t, ^3J(F,F) = 20.9 Hz, 1F; *para*-F), −157.1 (br. s, 2F; *β-pyrr*-F), −148.0 (d, 4.7 Hz, 2F; *β-pyrr*-F), −157.8 (d, 4.7 Hz, 2F; *β-pyrr*-F), −163.6 (br. s, 2F; *β-pyrr*-F), −164.0 (dt, ^3J(F,F) = 23.7 Hz, ^4J(F,F) = 7.7 Hz, 4F; *meta*-F), −164.5 (dt, ^3J(F,F) = 24.3 Hz, ^4J(F,F) = 7.7 Hz, 2F; *meta*-F).

It was difficult to get a pure product (as indicated by TLC), and the almost pure product was used for cobalt metalation.

Synthesis of Co−F_8. All the amount of the free base corrole that was obtained from the synthesis of 2,3,7,8,12,13,17,18-octafluoro-5,10,15-tris(pentafluorophenyl)corrole was collected and redissolved in 20 mL of pyridine. A 100 mg portion of $Co(OAc)_2{\cdot}4H_2O$ (0.40 mmol) was added, and the solution was heated to reflux for 20 min. The reaction progress was monitored by TLC examination (silica, CH_2Cl_2/*n*-hexane 1:1), and it was stopped when the fluorescent band of the free base corrole disappeared and the red and nonfluorescent band of the cobalt corrole appeared. The solvent was removed under vacuum, and Co−F_8 was isolated as the major product by column chromatography on silica gel 60 (eluent: CH_2Cl_2/hexanes/pyridine 2:1:0.001). Solvent evaporations and recrystallization from CH_2Cl_2/*n*-hexane mixtures resulted in 50 mg (43.3 μmol, 4.0% yield from the starting amount of the aldehyde) of Co−F_8 as red crystals. ^{19}F NMR (565 MHz, C_6D_6): δ, ppm= −140.7 (dd, ^3J(F,F) = 24.3 Hz, ^4J(F,F) = 7.9 Hz, 2F; *ortho*-F), −140.9 (dd, ^3J(F,F) = 24.3 Hz, ^4J(F,F) = 7.9 Hz, 4F; *ortho*-F), −147.2 (d, 6.2 Hz, 2F; *β-pyrr*-F), −148.0 (d, 5.7 Hz, 2F; *β-pyrr*-F), −149.2 (d, 6.2 Hz, 2F; *β-pyrr*-F), −151.1 (t, ^3J(F,F) = 20.1 Hz, 2F; *para*-F), −151.9 (t, ^3J(F,F) = 22.0 Hz, 1F; *para*-F), −153.8 (d, 6.2 Hz, 2F; *β-pyrr*-F), −162.6 (dt, ^3J(F,F) = 24.3 Hz, ^4J(F,F) = 7.9 Hz, 4F; *meta*-F), −163.3 (dt, ^3J(F,F) = 24.3 Hz, ^4J(F,F) = 7.0 Hz, 2F; *meta*-F). ^{1}H NMR (200 MHz, C_6D_6): δ, ppm= 4.92 (t, 6.4 Hz, 2 H; *para*-H of pyridine), 4.2 (t, 6.2 Hz, 4H; *meta*-H of pyridine), 1.34 (br. s, 4H; *ortho*-H of pyridine). UV/vis (benzene): λ_{max}, nm (ε, M^{-1} cm^{-1}) = 418 (1.17 × 10^6), 563 (3.00 × 10^5). HR(ESI)-MS in negative ion mode (M^-) (M-2pyridine = $C_{37}N_4F_{15}F_8Co$): calcd. for *m*/*z* = 995.9088, obsd. 995.9085 (100%). X-ray quality crystals of Co−F_8 were obtained by slow recrystallization from mixtures of benzene/*n*-heptane (1:1).

4. Density Functional Theory Calculations. All of the calculations were performed on the Inorganic-HPC cluster at IACS using the Gaussian 03 software package. The geometries were optimized with the spin-unrestricted formalism using both the BP86 functionals and the 6-311G* basis set for Co and 6-31G* basis set for other atoms.

dx.doi.org/10.1021/ic4000473 | *Inorg. Chem.* 2013, 52, 3381−3387

Frequency calculations were performed on each optimized structure using the same basis set to ensure that it was a minimum on the potential energy surface. Total energy calculations were performed using the 6-311+G* basis set in water solvent and a convergence criterion of 10^{-10} hartree. Basis-set superposition error has been reported to be minimal (~1 kcal/mol) for anion binding at this level of theory.

3. RESULTS AND ANALYSIS

In our pursuit of an efficient catalyst that can generate H_2 from H_2O electrochemically, we decided to focus on the Co complex of fully fluorinated corrole, which was prepared via metalation of the already reported macrocycle.[21] Co−F_8 was isolated as the bis-pyridine complex, and its characterization by X-ray crystallography (Supporting Information, Figure S9) revealed quite a perfectly planar macrocycle.[22] Conventional corroles are very electron-rich ligands that stabilize metals in high oxidation states,[23] while the reactivity of low-valent metallocorroles (i.e., in <2+ oxidation states) has not been thoroughly explored.[24−30] Recent investigations have however revealed that halogenation of the eight β-pyrroles in corroles affects the redox properties of the chelated transition metal ion much more dramatically than in other related macrocycles. This is attributed to the fact that halogenation of corroles (as in Co−F_8) does not induce structural deformations that attenuate the electron withdrawing effect of the substituents.[31] Cyclic voltammetry (CV, Figure 1b) of the Co−F_8 in a degassed acetonitrile solution displays a reversible Co(II/I) redox couple at −0.97 V (Figure 1b, blue), almost half a volt more positive than for the nonfluorinated analogue.[32] A large electrocatalytic current was observed when the CV of Co−F_8 was performed in the presence of an acid (0.13 M trifluoroacetic acid (TFA) (Figure 1b, red), which is ascribed to H_2 formation. Spectro-electrochemistry (Supporting Information, Figure S1, S2) of the Co−F_8 complex in acetonitrile reveals that it is reduced to its Co(I) state at −0.97 V, which is the active form for HER catalysis.

Keeping in mind the goal of HER catalysis in aqueous environments, Co−F_8 was physiabsorbed onto an edge-plane pyrolytic graphite (EPG) electrode, thus allowing for electrochemical investigations of this water-insoluble catalyst in aqueous solutions under heterogeneous conditions. The CV of the Co−F_8 catalyst immobilized on EPG in a pH 7 buffer solution shows that the Co(II/I) couple has shifted to −0.38 V vs Ag/AgCl in aqueous medium relative to −0.97 V vs Ag/AgCl in acetonitrile (Supporting Information, Figure S3). This may possibly be attributed to the greater ability of water to solvate the doubly reduced $[Co(I)\text{-corrole}]^{2-}$ complex (note that the corrole donates 3 negative charges).[33] The positive shift in the Co(II/I) potential is very encouraging regarding H_2 generation at relatively low overpotential.

Strong indication for H_2 production was obtained by a linear sweep voltammetry (LSV) experiment. When the potential of the Co−F_8 catalyst bearing the EPG electrode was lowered below the Co(II/I) redox couple in a 0.5 M H_2SO_4 solution, a large electrocatalytic current started to grow (Figure 2a, red) with concomitant gas bubble formation on the surface of the electrode (Figure 2b). The onset potential of this current, indicated by a 10-fold increase of the current with respect to bare EPG, was at about −0.5 V vs Ag/AgCl (Figure 2a, orange). This implies that catalysis is intimately correlated with the reduction of Co(II) to Co(I) in the aqueous acidic solution. Pronounced catalytic currents were also observed (Figure 2a, blue) with catalyst physiabsorbed on an Au electrode bearing a self-assembled monolayer (SAM) of octanethiol. Thus the catalyst is capable of HER when physiabsorbed on graphite as well as SAM covered Au/Ag electrodes. This is important for in situ investigations of the catalyst structure under H_2 forming conditions (vide infra) using Surface Enhanced Resonance Raman spectroscopy (SERRS) which can only be performed on SAM covered Au/Ag electrodes and not on EPG electrodes.

Evolution of H_2 was confirmed on both the EPG and Au-SAM electrodes (Figure 2c), using the rotating ring disc electrochemistry (RRDE) technique.[34] The disc bearing the catalyst was rotated at a steady rate that ensures that the hydrodynamic current produced due to the rotation of the electrode removes any H_2 produced on the disc away from it radially. The Pt ring that encircles the disc electrode was held at an oxidizing potential (0.7 V vs Ag/AgCl), which oxidizes the H_2 back to H^+ and produces a ring current (Supporting Information, Figure S4).[10] The selective detection of H_2 formation by the ring current confirmed that the onset of H_2 production by Co−F_8 is −0.5 V (−0.3 V vs NHE) on the EPG electrode and −0.3 V (−0.1 V vs NHE) on the Au-SAM electrode.

The reaction was elucidated to be first order with respect to the H^+ concentration (Supporting Information, Figure S5). This implies that the ratio $i_{cat}/[\tau]$, between the catalytic current obtained in the presence of substrate (i_{cat}) and the polarographic charge ($[\tau]$) is a measure of the TOF. The TOF in 0.5 M H_2SO_4 under anaerobic condition at room temperature and at −0.7 V and −0.8 V was determined to be 600 s^{-1} and 1140 s^{-1}, respectively. Electrolysis under anaerobic condition at −0.8 V revealed no decay in the catalyst activity (Figure 2d) for up to 16 h. During this process, 32.16 C was dissipated from the electrode bearing $4 \pm 0.2 \times 10^{-11}$ moles of Co−F_8 (obtained from integration of the CV current).[35] This indicates that the TON of the catalyst is $\gg 10^7$.

For in situ investigations of the electro-active species involved in catalysis during an RRDE experiment under H_2 forming conditions we turned our attention to the Surface Enhanced Resonance Raman Spectroscopy on Rotating Disc Electrode (SERRS-RDE) setup. SERRS-RDE of the Co−F_8 compound absorbed on octanethiol SAM on a roughened Ag disc[36a] that was held at 0 V (i.e., when there is no significant H_2 production) in a pH 7 buffer solution shows a spectrum very similar to that of the Co−F_8 complex in solution (Figure 3a). The vibrations of the Co(II) corrole complex (1350−1400 cm^{-1} and 1530−1580 cm^{-1} region) were observed on the SAM surface at similar energies and with intensities similar to those observed for the catalyst in acetonitrile solution. This confirms the presence of an intact Co−F_8 catalyst on the electrode after immobilization. Lowering the potential to −0.6 V in a pH 7 buffer solution, where normally H_2 is produced from acidic solutions, caused significant changes in the spectrum in the 300−500 cm^{-1} region. Although the oxidation and spin state marker bands of Co corroles have not been identified/defined (unlike their porphyrin counterparts), the band at 343 cm^{-1} shifts to 341 cm^{-1} and loses intensity relative to the band at 385 cm^{-1} (Figure 3b). Identical changes were observed when the Co center in the Co−F_8 complex was reduced to its +1 state by bulk electrolysis at −1 V in acetonitrile (Figure 3c). These observations indicate that the active form of the catalyst in pH 7 at −0.6 V (i.e., at the potential where H_2 is produced on SAM as well as EPG surfaces from acidic water) has the Co ion in its +1 oxidation state.[36b] In other words, the SERRS-RDE data indicate that the active catalyst on

dx.doi.org/10.1021/ic4000473 | Inorg. Chem. 2013, 52, 3381−3387

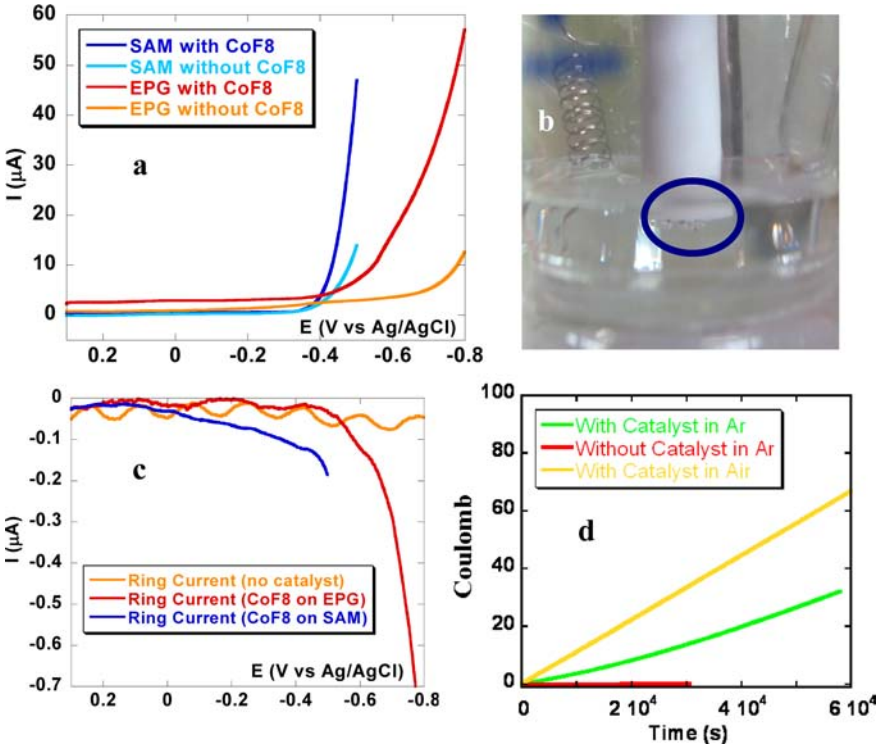

Figure 2. (a) LSV of EPG with catalyst (red), EPG without catalyst (orange), SAM with catalyst (blue) and SAM without catalyst (cyan). (b) Bubbles formed (highlighted by the blue circle) on the EPG electrode containing the catalyst after a LSV run. (c) Ring currents generated in RRDE experiments with electrodes having no catalyst (orange), with catalyst on EPG (red), and with catalyst on SAM (blue). All the experiments were done in deoxygenated 0.5 M H_2SO_4, using Ag/AgCl as reference, Pt wire as counter electrodes, and scan rate of 50 mV/s. (d) Plot of the current obtained at −0.8 V during ∼16 h of electrolysis of EPG with catalyst under aerobic condition (yellow), under Ar atmosphere (green), and without catalyst under Ar atmosphere (red).

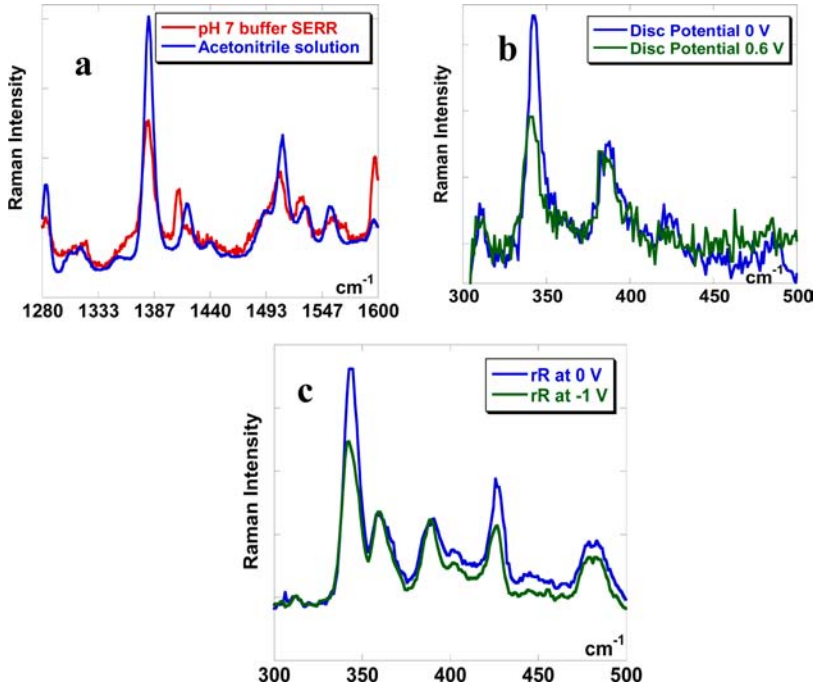

Figure 3. (a) Resonance Raman spectra of Co−F_8 electrolyzed at 0 V in acetonitrile (blue), i.e., homogeneous phase and on SAM surface in pH 7 (red). (b) SERRS-RDE data of the catalyst physiabsorbed on the SAM on a roughened Ag disc while electrolyzing it at 0 V (blue) and at −0.6 V (green). (c) Resonance Raman data of the compound in acetonitrile after electrolyzing it at 0 V (blue) and at −1 V (green).

the SAM surface is Co(I)−F_8, similar to the active catalyst under homogeneous conditions.

Encouraged by the results obtained with the Co−F_8 catalyst so far, we decided to confront another long-standing

dx.doi.org/10.1021/ic4000473 | Inorg. Chem. 2013, 52, 3381−3387

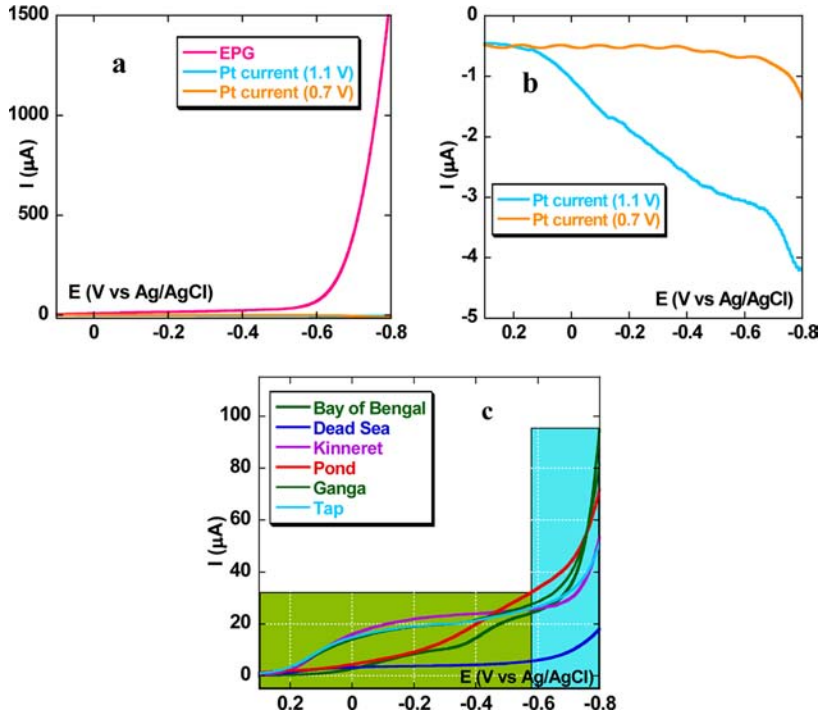

Figure 4. (a) RRDE results of the catalyst on EPG in air saturated 0.5 M H_2SO_4 showing EPG current (pink), Pt current when ring held at 1.1 V (cyan), and Pt current when ring held at 0.7 V (orange). (b) Enlarged view showing the Pt ring currents. (c) Electrochemical hydrogen production by the catalyst on EPG from H_2O obtained from local water bodies in India and Israel. Ag/AgCl and Pt wire were used as reference and counter electrodes respectively.

challenge: to catalyze the formation of H_2 from H^+ in the presence of O_2. To the best of our knowledge, only some Se-containing naturally occurring hydrogenases and one most recently reported molecular cobalt catalyst are capable of performing that task.[11b,37] The difficulty arises from the fact that any metal-based catalyst capable of generating H_2 from H^+ also readily reacts with O_2. This is why almost all H_2 evolution experiments, including the ones reported in this study up to here, were performed under strictly anaerobic conditions. In fact, the octabromo analogue of Co−F_8 catalyst has recently been demonstrated to be an excellent O_2 reducing electrocatalyst.[38] It is hence not surprising that the LSV of the Co−F_8 catalyst in air saturated 0.5 M H_2SO_4 shows a strong O_2 reduction current at 0.2 V (Figure 4a, pink), a potential where the Co(III) is reduced to Co(II) in acidic medium (Supporting Information, Figure S3). Clearly, the Co(II) generated on the electrode reduces O_2 present in the solution. There was however a further increase in the current as the potential was swept more negative (Figure 4a, pink). To elucidate the chemistry behind these observations, the Pt ring was poised at 1.1 V, revealing that current increased at around the same potential where O_2 reduction starts (Figure 4b, cyan). The Pt ring oxidizes H_2O_2 and O_2^- to O_2, as well as H_2 to H^+ at this potential. But since there was no current on either of the disc or the ring at these potentials in the absence of O_2 in the medium (see Figure 2a), the current detected at the Pt ring is due to oxidation of H_2O_2 produced by incomplete reduction of O_2 in acidic/areobic solutions. The further increase in the ring current below −0.6 V, when the Co(II) is reduced to Co(I), might in principle imply either greater H_2O_2 production by Co(I) relative to Co(II) or H_2 generation by Co(I) in addition to reduction of O_2. Holding the ring potential (at otherwise identical experimental conditions) at 0.7 V vs Ag/AgCl, conditions at which Pt oxidizes H_2 to H^+ but not H_2O_2 to O_2, allowed for the distinction between these two possibilities. No current was detected in the ring at potentials where an O_2 reduction current was observed in the disc (i.e., starting at 0.2 V), but only at potentials lower than −0.6 V (Figure 4b, orange). The experiments performed in the absence of O_2 thus indicate that H_2 is formed on the electrode at these potentials and is detected in the Pt ring when it is held at 0.7 V. We hence conclude that the Co−F_8 catalyst catalyzes H_2 formation from H^+ even in the presence of O_2.

The stability and performance of the catalyst under aerobic conditions may not be assessed by $i_{cat}/[\tau]$, since the i_{cat} represents both O_2 and H^+ reduction currents and the $[\tau]$ is enveloped by the O_2 reduction current. Catalyst immobilized on EPG was able to electrolyze an aerated 0.5 M H_2SO_4 solution over a period of 16 h, and no decay of the catalytic current was observed (Figure 2d, yellow). However, the total number of coulombs dissipated was two times the value dissipated under anaerobic conditions (Figure 2d, green). The Faradaic yield (FY) under aerobic conditions was evaluated by measuring the volume of H_2 liberated during electrolysis using an inverted buret setup (Supporting Information, Figure S7a). The results were quite revealing: 9.1 mL of H_2 were evolved and 149 C of charge dissipated from the electrode after 10 h of electrolysis in an aerobic 0.5 M H_2SO_4 solution (Supporting Information, Figure S7b). This implies that the FY for H_2 production at −0.8 V in 0.5 M H_2SO_4 is 52%. For comparison, the sole catalyst that has been demonstrated to work under aerobic conditions provided a FY of 45% and TOF of 0.0042 s^{-1}.[11b] Most importantly SERRS experiments performed before and after H_2 evolution indicate that the Co−F_8 catalyst stays intact on the electrode (Supporting Information, Figure S6) and does not

dx.doi.org/10.1021/ic4000473 | Inorg. Chem. 2013, 52, 3381−3387

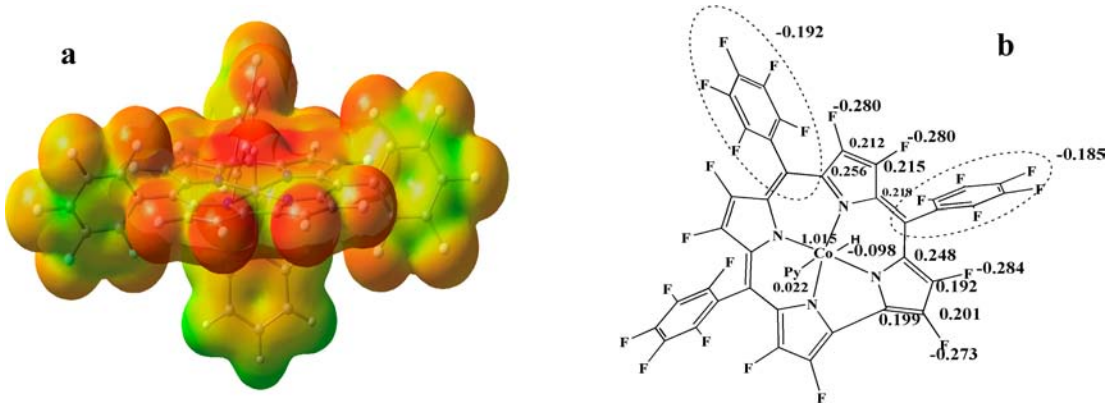

Figure 5. (A) Calculated electrostatic potential of the $[Co(III)\text{-}H]^-$ species, and (B) the calculated Mulliken population of the $[Co(III)\text{-}H]^-$ species.

decay as has been reported to be the case for some other Co catalysts.[20]

Another aspect that increases the maintenance cost and decreases the applicability of a practical H_2 generation setup is the requirement for a clean water source, which is a common practice in research but not in real life. We have thus investigated the ability of Co−F_8 immobilized on EPG to generate H_2 from various available water sources, in contrast to the triply distilled H_2O used up to here. In all these cases the water was filtered through a laboratory filter paper followed by addition of H_2SO_4 to attain a final concentration of 0.5 M. No other chemical or physical treatments were used. Water from tap water, a local pond (IACS), the Ganges (delta region, high saline content and silt and industrial waste contaminated), the Bay of Bengal (saline and silt bearing), the Dead Sea (most saline containing natural H_2O source), and the Sea of Galilee (natural fresh water lake) were used. The data from all the water sources show that both O_2 reduction current (below 0.2 V, Figure 4c green region) and H^+ reduction current (below −0.6 V, H_2 detected in situ using Pt ring, Figure 4c cyan region) are present. The amount of H_2 generated from all water sources, except that obtained from the Dead Sea was significant, which demonstrates that Co−F_8 is an efficient HER catalyst under truly reasonable conditions.

The spectroscopic data suggest Co(I) to be the active form of the catalyst. Additionally, the potential for H^+ reduction coincides with the Co(II/I) reduction indicating that Co(I) is the reactive species. The linear dependence of the catalytic current on proton concentration (Supporting Information, Figure S5) indicates that the reaction follows first order kinetics with respect to $[H]^+$. Also a substrate diffusion limited current is not observed; rather, a kinetic barrier in the catalysis seems to determine the electrocatalytic current. Taken together these facts suggest the following mechanism for H_2 generation.[39]

$$[Co(I)]^{-2} + H^+ \rightarrow [Co(III)\text{−}H]^- + H^+ \rightarrow Co(III) + H_2$$

Geometry optimized density functional theory (DFT) calculations are performed to evaluate the feasibility of this process. The calculated free energies reflect that the reduction to Co(II) to Co(I) is the most thermodynamically uphill step with a ΔG of +25.74 kCal/mol. This translates into a reduction potential of −1.1 eV. The protonation of the Co(I) species to generate a $[Co(III)\text{-}H]^-$ species and the subsequent protonation of the $[Co(III)\text{-}H]^-$ species to release H_2 and result in the oxidation of Co(I) to Co(III) are calculated to be energetically favorable. Interestingly, while the protonation of the Co(I) species is energetically favorable, the protonation of the $[Co(III)\text{-}H]^-$ is not. The calculated electrostatic potential map (Figure 5A) of this species indicates that the accumulated anionic charge density on the H^- species is small, and the corresponding Mulliken charge (Figure 5B) on H is calculated to be ∼ −0.1. Alternatively, significant electron density is observed on the fluoride substituents of the corrole ring indicating charge delocalization off the H atom into the macrocycle. This leads to weaker protonation energy (i.e., lower pK_a) of this H^- to liberate H_2. Taken together, the linear dependence of the catalytic current with $[H^+]$ (indicating that the rds involved protonation), the calculated free energy of protonation, and the ground state electronic structure of the $[Co(III)\text{-}H]^-$ species suggest that the protonation of the $[Co(III)\text{-}H]^-$ species is the rds for this catalyst (Scheme 1).

Scheme 1. Mechanism for H_2 Evolution Catalyzed by a Molecular Cobalt Corrole Complex

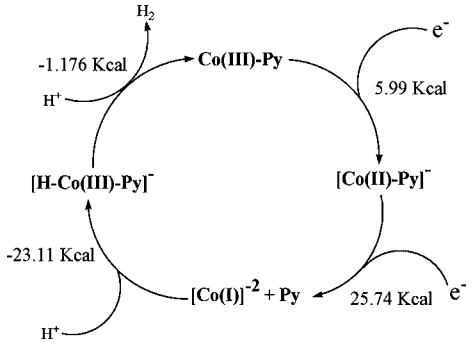

6. CONCLUSION

In summary, we report a Co-based electrocatalyst that can reduce H^+ from H_2O to form H_2 with an onset at −0.3 V vs NHE on a graphite electrode and close to its thermodynamic potential on a thiol monolayer covered Au electrode (onset at −0.1 V vs NHE). In situ SERRS confirms successful immobilization of the intact catalyst on electrodes and further indicates that the Co in Co−F8 is reduced to Co(I) at potentials where it produces H_2. The catalyst has a turnover frequency of 600 s^{-1} at −0.5 V vs NHE in 0.5 M H_2SO_4 and a turnover number of $\gg 10^7$. It is also capable of reducing H_2 in the presence of O_2 with a FY of 52% and TON comparable to those observed under anaerobic conditions. An additional feature is that the Co−F_8 catalyst is capable of producing H_2

dx.doi.org/10.1021/ic4000473 | Inorg. Chem. 2013, 52, 3381−3387

from a variety of local and global water sources without the need for any pretreatment. Electronic structure calculations and $[H]^+$ dependence of the catalytic activity suggests that the protonation of a putative $[Co(III)\text{-}H]^-$ species is the rds of the HER catalyzed by this complex.

■ ASSOCIATED CONTENT

Supporting Information

Crystallographic data, absorption, and EPR spectra of the complex related to catalysis, experiments related to H_2 detection and quantification, and related electrochemical data. This material is available free of charge via the Internet at http://pubs.acs.org.

■ AUTHOR INFORMATION

Corresponding Author

*E-mail: icsgd@iacs.res.in (S.G.D.), chr10zg@tx.technion.ac.il (Z.G.), icad@iacs.res.in (A.D.).

Notes

The authors declare no competing financial interest.

■ ACKNOWLEDGMENTS

The research was funded by DST Grant DST/SR/IC-35-2009 (A.D.) and BRNS Grant 2011/36/12-BRNS (A.D. and S.G.D.) and the GTEP-RBNI Nevet grant (Z.G.). B.M. acknowledges CSIR-SPM-JRF and K.S. acknowledges CSIR-SRF. Work at the Technion was supported by the Grand Technion Energy Program (GTEP).

■ REFERENCES

(1) Cook, T. R.; Dogutan, D. K.; Reece, S. Y.; Surendranath, Y.; Teets, S. T.; Nocera, D. G. *Chem. Rev.* **2010**, *110*, 6474−6502.

(2) Lubitz, W.; Tumas, W. *Chem. Rev.* **2007**, *107*, 3900−3903.

(3) Esswein, A. J.; Nocera, D. G. *Chem. Rev.* **2007**, *107*, 4022−4047.

(4) Holladay, J. D.; Wang, Y.; Jones, E. *Chem. Rev.* **2004**, *104*, 4767−4790.

(5) Kodama, T.; Gokon, N. *Chem. Rev.* **2007**, *107*, 4048−4077.

(6) R. M. Navarro, M. A.; Peña, J. L.; Fierro, G. *Chem. Rev.* **2007**, *107*, 3952−3991.

(7) Palo, D. R.; Dagle, R. A.; Holladay, J. D. *Chem. Rev.* **2007**, *107*, 3992−4021.

(8) Reece, S. Y.; Hamel, J. A.; Sung, K.; Jarvi, T. D.; Esswein, A. J.; Pipers, J. J. H.; Nocera, D. G. *Science* **2011**, *334*, 645−648.

(9) Du, P.; Eisenberg, R. *Energy Environ. Sci.* **2012**, *5*, 6012−6021.

(10) Le Goff, A.; Artero, V.; Jousselme, B.; Tran, P. D.; Guillet, N.; Metaye, R.; Fihr, A.; Palacin, S.; Fontecave, M. *Science* **2009**, *326*, 1384−1387.

(11) (a) Helm, M. L.; Stewart, M. P.; Bullock, R. M.; DuBois, M. R.; DuBois, D. L. *Science* **2011**, *333*, 863−866. (b) Lakadamyali, F.; Kato, M.; Muresan, N. M.; Reisner, E. *Angew. Chem., Int. Ed.* **2012**, *51*, 9381−9384. (c) Singh, W. M.; Baine, T.; Kudo, S.; Tian, S.; Na, X. A. N.; Zhou, H.; DeYonker, N. J.; Pham, T. C.; Bollinger, J. C.; Baker, D. L.; Yan, B.; Webster, C. E.; Zhao, X. *Angew. Chem., Int. Ed.* **2012**, *51*, 5941−5944. (d) Lee, C. H.; Dogutan, D. K.; Nocera, D. G. *J. Am. Chem. Soc.* **2011**, *133*, 8775−8777. (e) Roubelakis, M. M.; Bediako, D. K.; Dogutan, D. K.; Nocera, D. G. *Energy Environ. Science* **2012**, *5*, 7737−7740.

(12) (a) Baffert, C.; Artero, V.; Fontecave, M. *Inorg. Chem.* **2007**, *46*, 1817−1824. (b) Razavet, M.; Artero, V.; Fontecave, M. *Inorg. Chem.* **2005**, *44*, 4786−4795. (c) McCormick, T. M.; Han, Z.; Weinberg, D. J.; Brennessel, W. W.; Holland, P. L.; Eisenberg, R. *Inorg. Chem.* **2011**, *50*, 10660−10666.

(13) (a) Rose, M. J.; Gray, H. B.; Winkler, J. R. *J. Am. Chem. Soc.* **2012**, *134*, 8310−8313. (b) McNamara, W. R.; Han, Z.; Alperin, P. J.; Brennessel, W. W.; Holland, P. L.; Eisenberg, R. *J. Am. Chem. Soc.* **2011**, *133*, 15368−15371. (c) Han, Z.; McNamara, W. R.; Eum, M. S.; Holland, P. L.; Eisenberg, R. *Angew. Chem., Int. Ed.* **2012**, *51*, 1667−1670.

(14) Karunadasa, H. I.; Chang, C. J.; Long, J. R. *Nature* **2010**, *464*, 1329−1333.

(15) Karunadasa, H. I.; Montalvo, E.; Sun, Y.; Majda, M.; Long, J. R.; Chang, C. J. *Science* **2012**, *335*, 698−702.

(16) Sun, Y.; Bigi, J. P.; Piro, N. A.; Tang, M. L.; Long, J. R.; Chang, C. J. *J. Am. Chem. Soc.* **2011**, *133*, 9212−9215.

(17) McCrory, C. C. L.; Uyeda, C.; Peters, J. C. *J. Am. Chem. Soc.* **2012**, *134*, 3164−3170.

(18) Berben, L. A.; Peters, J. C. *Chem. Commun.* **2010**, *46*, 398−400.

(19) Stubbert, B. D.; Peters, J. C.; Gray, H. B. *J. Am. Chem. Soc.* **2011**, *133*, 18070−18073.

(20) Anxolabéhère-Mallart, E.; Costentin, C.; Fournier, M.; Nowak, S.; Robert, M.; Savéant, J. M. *J. Am. Chem. Soc.* **2012**, *134*, 6104−6107.

(21) Lui, H. Y.; Lai, T. S.; Yeung, L. L.; Chang, C. K. *Org. Lett.* **2003**, *5*, 617−620.

(22) CCDC 893235 contains the supplementary crystallographic data for Co-F_8. This data can be obtained free of charge from The Crystallographic Data Centre via www.ccdc.cam.ac.uk/data_request/cif.

(23) (a) Watanabe, Y. In *Porphyrin Handbook*; Kadish, K. M., Kevin, S. M., Guilard, R., Eds.; Academic Press: New York, 2000;, Vol. *4*, pp 97−117. (b) Guildard, R.; Barbe, J. M.; Stern, C.; Kadish, K. M. In *Porphyrin Handbook*; Kadish, K. M., Kevin, S. M., Guilard, R., Eds.; Academic Press: New York, 2003; Vol. *18*, pp 303−349.

(24) Gross, Z. *J. Biol. Inorg. Chem.* **2001**, *6*, 733−738.

(25) Aviv, I.; Gross, Z. *Chem. Commun.* **2007**, 1987−1999.

(26) Abu-Omar, M. M. *Dalton. Trans.* **2011**, *40*, 3435−3444.

(27) Will, S.; Lex, J.; Vogel, E.; Adamian, V. A.; Caemelbecke, E. V.; Kadish, K. M. *Inorg. Chem.* **1996**, *35*, 5577−5583.

(28) Ghosh, A.; Wondimagegn, T.; Parusel, A. B. J. *J. Am. Chem. Soc.* **2000**, *122*, 5100−5104.

(29) Meier-Callahan, A. E.; Gray, H. B.; Gross, Z. *Inorg. Chem.* **2000**, *39*, 3605−3607.

(30) Gross, Z.; Gray, H. B. *Inorg. Chem.* **2006**, *27*, 61−72.

(31) (a) Mahammed, A.; Timanskii, B.; Gross, Z. *J. Porphyrins Phthalocyanines* **2011**, *15*, 1276. (b) Mahammed, A.; Botoshansky, M.; Gross, Z. *Dalton Trans.* **2012**, *41*, 10938−10940.

(32) Grodkowski, J.; Neta, P.; Fujita, E.; Mahammed, A.; Simkhovich, L.; Gross, Z. *J. Phys. Chem. A* **2002**, *106*, 4772−4778.

(33) (a) Barker, J. D.; Eckermann, A. L.; Sazinsky, M. H.; Hartings, M. R.; Abajian, C.; Georganopulou, D.; Ratner, M. A.; Rosenzweig, A. C.; Meade, T. J. *Bioconjugate Chem.* **2009**, *20*, 1930−1939. (b) Dey, A.; Jenney, F. E.; Adams, M. W. W.; Babini, E.; Takahashi, Y.; Fukuyama, K.; Hodgson, K. O.; Hedman, B.; Solomon, E. I. *Science* **2007**, *318*, 1464−1468.

(34) Bard, A. J.; Faulkner, L. R. *Electrochemical Methods*; J. Wiley: New York, 1980.

(35) Note that while the CV current is weak, it yields the same coverage over various scan rates, Supporting Information, Figure S10.

(36) (a) Both Ag and Au form stable monolayers with thiols and can physiabsorb the Co-F_8 catalyst, but only Ag can be used as SERRS substrate for 413.1 nm excitation into the Soret band of Co-F_8. (b) We assume that inferences based on the spectroscopic data obtained on the SAM covered Ag electrode is also applicable to SAM covered Au electrode and EPG electrodes.

(37) Parkin, A.; Goldet, G.; Cavazza, C.; Fontecilla-Camps, J. C.; Armstrong, F. A. *J. Am. Chem. Soc.* **2008**, *130*, 13410−13426.

(38) Schechter, A.; Stanevsky, M.; Mahammed, A.; Gross, Z. *Inorg. Chem.* **2011**, *51*, 22−24.

(39) (a) Kellet, R. M.; Spiro, T. G. *Inorg. Chem.* **1985**, *24*, 2373−2377. (b) Marinescu, S. C.; Winkler, J. R.; Gray, H. B. *Proc. Natl. Acad. Sci. U.S.A.* **2012**, *109*, 15127−15131.